EPJ Quantum Technology
a SpringerOpen Journal

RESEARCH   **Open Access**

Efficient quantum state estimation with low-rank matrix completion

Shehbaz Tariq[1†], Ahmad Farooq[1,2†], Junaid Ur Rehman[3], Trung Q. Duong[4] and Hyundong Shin[1*]

[*]Correspondence: hshin@khu.ac.kr
[1]Department of Electronics and Information Convergence Engineering, Kyung Hee University, 1732 Deogyeong-daero, Yongin-si, Gyeonggi-do 17104, Korea
Full list of author information is available at the end of the article
[†]Equal contributors

Abstract

This paper introduces a novel and efficient technique for quantum state estimation, coined as low-rank matrix-completion quantum state tomography for characterizing pure quantum states, as it requires only non-entangling bases and $2n + 1$ local Pauli operators. This significantly reduces the complexity of the process and increases the accuracy of the state estimation, as it eliminates the need for the entangling bases, which are experimentally difficult to implement on quantum devices. The required minimal post-processing, improved accuracy and efficacy of this matrix-completion-based method make it an ideal benchmarking tool for investigating the properties of quantum systems, enabling researchers to verify the accuracy of quantum devices, characterize their performance, and explore the underlying physics of quantum phenomena. Our numerical results demonstrate that this method outperforms contemporary techniques in its ability to accurately reconstruct multi-qubit quantum states on real quantum devices, making it an invaluable contribution to the field of quantum state characterization and an essential step toward the reliable deployment of intermediate- and large-scale quantum devices.

Keywords: NISQ; Quantum state tomography; Singular value decomposition; Fidelity; Matrix completion; Pauli operators

1 Introduction

Noisy intermediate-scale quantum (NISQ) devices consisting of hundreds of qubits will be available soon [1]. Several technologies for these NISQ devices are being pursued such as superconducting quantum circuits [2], trapped ions [3], quantum dot [4], cold atoms [5], and photonic platforms [6]. These NISQ computers are expected to perform tasks that surpass the capability of the most powerful classical computers available today [7–9]. However, noisy quantum gates and decoherence limits the desired level of improvement over the existing current classical computing devices for complex algorithms. Bearing this in mind, the development of NISQ devices has posed a paradox: how to validate that the device produces the desired result? For characterization, certification, and benchmarking [10] of these noisy devices, quantum state tomography comes into play, which is the gold standard for the reconstruction of a quantum state [11]. Reconstruction of the quantum

Springer

state from measurements on the replica of an unknown given quantum state is termed as the quantum state tomography. Quantum state tomography generally consists of a two-step process: the first is collecting the data from optimized measurement design on quantum systems; the second is the classical post-processing of the gathered data. Quantum state tomography problem becomes intractable due to an exponential growth of the system size with increase in the number of qubits under consideration [12, 13].
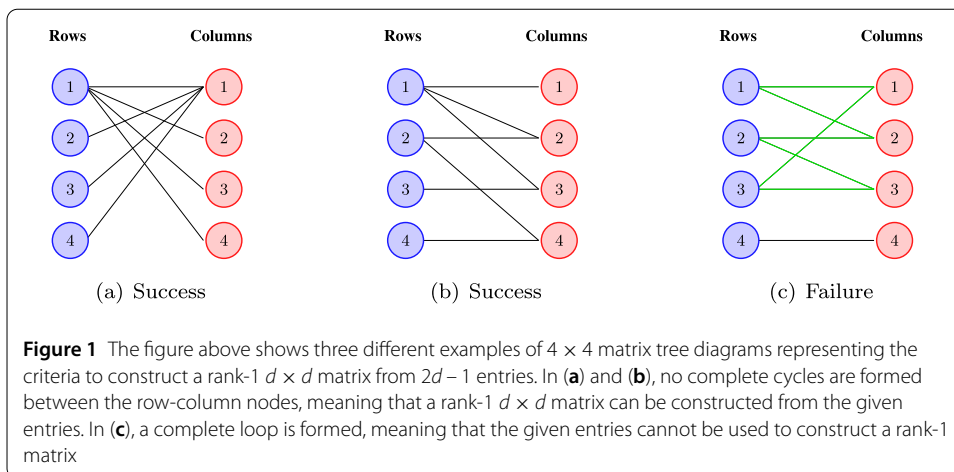
A conventional state standard tomography employs d^2 or more measurement settings, where $d = 2^n$ for n qubits [14–17]. A simple counting argument suggests that only $O(d)$ measurement settings are sufficient to perform the tomography of pure quantum states [18, 19]. Compressed sensing and low-rank matrix recovery from sparse matrix algorithms have been developed to achieve this bound [20–22]. In [23, 24], the authors proposed $d + 1$ mutually unbiased bases measurements for *full* quantum state reconstruction. The states with special properties, for instance, matrix product states [25] or permutationally invariant quantum states [26] also lead to a significant reduction in the number of quantum measurement settings. The pure quantum state can also be retrieved with only five and three measurement settings given in [27–29]. Recently, noise resilient and robust self-guided quantum state tomography is proposed [30–32].

The use of entangled bases in most of the aforementioned tomography algorithms is common, however, their implementation on NISQ devices is difficult due to errors introduced by the controlled-NOT (CNOT) gate and the high circuit depth leading to qubit decoherence. The CNOT gate is an essential transformation required for implementing these sets of entangled measurements. Hence, these entangled bases significantly reduce the performance of state estimation task. The introduction of local basis measurement for state reconstruction can be a massive catalyst for the benchmarking of quantum devices. For this purpose, local basis measurements are introduced in [33]. They have demonstrated the task of tomography of pure quantum state by using $kn + 1$ measurement bases, where $k \geq 2$. Their algorithm is based on solving several systems of linear equations. The required number of bases increases ($k > 2$) if the determinant of the linear system of equations vanishes. The performance is quite low as compared to the numerical results of entangled measurement algorithms. Given the rank of a quantum state, the projected least squares can be used to achieve higher accuracy with the minimum number of copies. However, this comes at the cost of the local Pauli basis measurement settings increasing exponentially. The success of tomography algorithms, therefore, relies on the efficient use of resources to balance accuracy, efficiency, and fidelity.

The paper proposes a novel approach to quantum state tomography called low-rank matrix-completion (LRMC) quantum state tomography. This approach allows for the estimation of pure quantum states with only a minimum of $2n + 1$ local Pauli measurements for an n-qubit state. The algorithm makes use of experimental measurements to provide the necessary density matrix elements and then uses singular value shrinkage to fill in the missing entries. The method outperforms the existing techniques, as illustrated by simulations and experiments, and is capable of accurately detecting pure states with computational basis and local Pauli measurements.

2 Method
The method used in this paper for pure quantum state tomography involves a matrix filling technique involving $2n + 1$ local measurements for an n-qubit system. This technique

Figure 1 The figure above shows three different examples of 4 × 4 matrix tree diagrams representing the criteria to construct a rank-1 $d \times d$ matrix from $2d - 1$ entries. In (**a**) and (**b**), no complete cycles are formed between the row-column nodes, meaning that a rank-1 $d \times d$ matrix can be constructed from the given entries. In (**c**), a complete loop is formed, meaning that the given entries cannot be used to construct a rank-1 matrix

utilizes the algorithm for low-rank matrix completion [34]. The algorithm begins by experimentally acquiring enough entries of the pure state's density matrix. This data is then used by the matrix completion algorithm to obtain the complete density matrix of the desired state using a rank-1 approximation.

Filling in the missing entries of a rank-1 matrix is directly connected to the problem of finding cycles in a graph [34]. The rank-1 matrix of dimension $d \times d$ can be completely reconstructed by knowing only $2d - 1$ entries of the matrix. These $2d - 1$ elements form a spanning tree in the row-column graph, as demonstrated in Fig. 1. The successful reconstruction of the missing entries of the given matrix depends on the tree reaching all nodes without forming a loop. If a loop exists in the row-column graph, then it is not possible to reconstruct the rank-1 matrix. However, if the $2d - 1$ entries of the matrix do not form a cycle, then we can optimally impute all the missing entries using matrix completion techniques.

In this paper, we use the rank shrinkage procedure known as the Eckart-Young theorem [35] to compute the rank-1 density matrix from less measurement setting. This theorem states that the best low-rank approximation of a given matrix can be achieved by taking its singular value decomposition (SVD) and preserving only the largest singular values and their respective singular vectors. For a matrix A, the rank-k approximation of A_k is obtained by retaining only the k largest singular values and their corresponding singular vectors:

$$A_k = \sum_{i=1}^{k} \lambda_i u_i v_i^{\dagger}, \tag{1}$$

where λ_i are the singular values, u_i and v_i are the corresponding left and right singular vectors. For any matrix A, its best rank-k approximation is given as

$$\|A - A_k\|_F \leq \|A - B\|_F, \tag{2}$$

where $\| \cdot \|_F$ is the Frobenius norm and B any rank-k matrix. This remarks that SVD also gives the best low rank approximation in spectral norm [36]. This technique find applications in data compression, noise reduction, and dimensionality reduction. In the context

of quantum state tomography, the theorem facilitates the reconstruction of best low-rank quantum states from incomplete measurements settings.

In our algorithm, we perform local Pauli measurements on each subsystem of multipartite pure quantum state. We first employ the computational basis measurement to obtain the diagonal elements of the unknown density matrix. Next, we measure n-qubit systems in Pauli measurement setting

$$\Lambda_j^i = \sigma_z^{\otimes i-1} \otimes \sigma_j^i \otimes \sigma_z^{\otimes n-i}. \tag{3}$$

Here, i denotes the qubits's index and j denotes the Pauli operator index, which can be either 1 or 2. The index i ranges $i = 1, 2, \ldots, n$, where $\sigma_j^i \in \{\sigma_1, \sigma_2\}$ represents Pauli X (σ_1) and Pauli Y (σ_2) matrices.

We begin by assuming that we have access to N copies of a n-qubit multipartite unknown pure state $\rho = |\psi\rangle \langle\psi|$. In the simulation presented in the following section, for the sake of simplicity, we allocate an equal number of copies for all measurement settings. Specifically, we measure each of the $2n + 1$ bases using $N/(2n + 1)$ shots. In the first step of our algorithm, we obtain the diagonal elements of ρ by measuring $N/(2n + 1)$ of its copies in the computational basis of the d-dimensional Hilbert space. From the measurement results, diagonal elements of ρ can be directly obtained as

$$\hat{\rho}_{i,i} = \frac{(2n + 1)N_i}{N}, \quad \text{for } i \in \mathbb{Q}_d, \tag{4}$$

where $\mathbb{Q}_d = \{0, 1, \ldots, d - 1\}$, N_i is the number of times measurement result corresponding to $|i\rangle$ was obtained in the first step and $\hat{\rho}$ denotes an estimate of ρ.

The off-diagonal element $\rho_{j,k}$ of ρ can be obtained by measuring it in the eigenbasis of Pauli operators pair Λ_1^i and Λ_2^i. This can be seen by first noticing that the eigenvectors of Λ_1^i and Λ_2^i are

$$|V_{1,\pm1}^{2^i\nu+\zeta, 2^i\nu+\zeta+2^{i-1}}\rangle = \frac{1}{\sqrt{2}}\left(|2^i\nu + \zeta\rangle \pm |2^i\nu + \zeta + 2^{i-1}\rangle\right) \tag{5}$$

$$|V_{2,\pm1}^{2^i\nu+\zeta, 2^i\nu+\zeta+2^{i-1}}\rangle = \frac{1}{\sqrt{2}}\left(|2^i\nu + \zeta\rangle \pm i|2^i\nu + \zeta + 2^{i-1}\rangle\right), \tag{6}$$

where $\nu \in \mathbb{Q}_{\frac{d}{2^i}}$, $\zeta \in \mathbb{Q}_{2^{i-1}}$ and the basis sets are constructed from all possible combinations of values in ν, ζ and i qubits.

These orthonormal bases build a complete projector system with elements

$$\Pi_{x,-1}^{j,k} = |V_{x,-1}^{j,k}\rangle \langle V_{x,-1}^{j,k}| \tag{7}$$

$$\Pi_{x,1}^{j,k} = |V_{x,1}^{j,k}\rangle \langle V_{x,1}^{j,k}|. \tag{8}$$

where $x \in \{1, 2\}$, $j = 2^i\nu + \zeta$ and $k = 2^i\nu + \zeta + 2^{i-1}$. Let $p_{x,m}^{j,k}$ be the probability of obtaining the measurement outcome corresponding to the projector $\Pi_{x,m}^{j,k}$. Then, we have

$$p_{1,-1}^{j,k} = \frac{1}{2}(\hat{\rho}_{j,j} - \hat{\rho}_{j,k} - \hat{\rho}_{k,j} + \hat{\rho}_{k,k}) \tag{9}$$

$$p_{1,1}^{j,k} = \frac{1}{2}(\hat{\rho}_{j,j} + \hat{\rho}_{j,k} + \hat{\rho}_{k,j} + \hat{\rho}_{k,k}) \tag{10}$$

$$p_{2,-1}^{j,k} = \frac{1}{2}(\hat{\rho}_{j,j} + i\hat{\rho}_{j,k} - i\hat{\rho}_{k,j} + \hat{\rho}_{k,k}) \tag{11}$$

$$p_{2,1}^{j,k} = \frac{1}{2}(\hat{\rho}_{j,j} - i\hat{\rho}_{j,k} + i\hat{\rho}_{k,j} + \hat{\rho}_{k,k}), \tag{12}$$

where $\hat{\rho}_{j,k} = \langle j|\rho|k\rangle$ is the element of ρ at (j,k)th index. From the hermiticity of ρ, we have $\rho_{k,j} = \rho_{j,k}^*$. Using this fact, we get $\rho_{j,k} + \rho_{k,j} = 2\operatorname{Re}\{\rho_{j,k}\}$ and $\rho_{j,k} - \rho_{k,j} = 2\operatorname{Im}\{\rho_{j,k}\}$. By subtracting equation (9) from (10) and equation (11) from (12), and then combining the results while utilizing the facts about the real and imaginary components of $\hat{\rho}_{j,k}$, we can derive the value of $\hat{\rho}_{j,k}$ as

$$\hat{\rho}_{j,k} = \frac{1}{2}\left(-p_{1,-1}^{jk} + p_{1,1}^{jk} - ip_{2,-1}^{jk} + ip_{2,1}^{jk}\right). \tag{13}$$

From $\hat{\rho}_{j,k}$, we can easily get $\hat{\rho}_{k,j} = \hat{\rho}_{j,k}^*$. This setup provides us with a sufficient number of elements to fill in the missing entries of the density matrix. Let $\hat{\rho}$ be $d \times d$ matrix containing all entries obtained from measurement operators along with missing entries at $(i,j) \in \Delta$, i.e.,

$$\Delta = \left\{(i,j) : \hat{\rho}_{i,j} \text{ is missing entry}\right\}. \tag{14}$$

Several methods exist for imputing missing entries in a density matrix, such as substituting them with zeros or calculating the average of the respective column or row. However, the choice of initial imputation is less critical since our algorithm will update only these missing values while preserving the values obtained from measurement operators [37, 38]. Let $\hat{\rho}_{.,j}$ denotes the j-th column of the density matrix $\hat{\rho}$. We calculate the missing entries by taking the average of the each column in the density matrix as

$$\hat{\rho}(\Delta) = \operatorname{mean}(\hat{\rho}_{.,j}), \quad \forall(i,j) \in \Delta. \tag{15}$$

We can also detect if an unknown quantum state is pure using our algorithm without the need for additional measurements. A density matrix ρ is considered pure if the equation
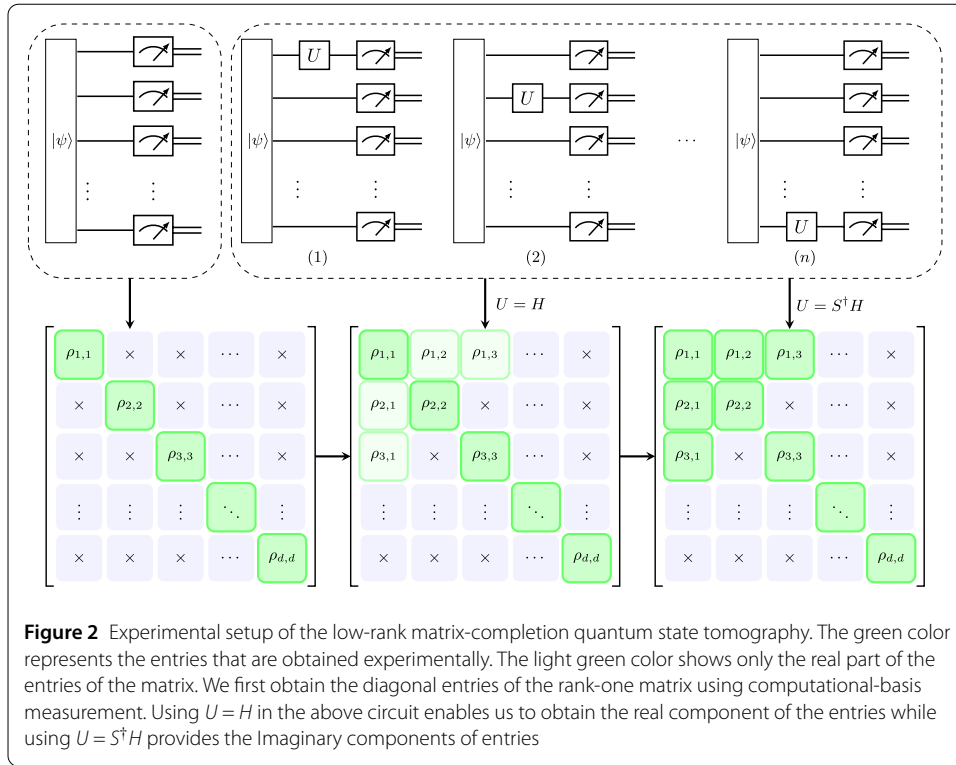
$$|\rho_{i,j}|^2 = |\rho_{i,i}||\rho_{j,j}| \tag{16}$$

holds for every $i,j = 1,2,\ldots,d$. We can verify the purity of the unknown state by using Equation (16) on the measured structure from Fig. 2 and applying it to elements of the constructed density matrix.

The complete algorithm for constructing the density matrix of a pure quantum state ρ is as follows:

1. Measure ρ in the computational basis to obtain the diagonal entries of the density matrix through Equation (4).
2. Obtain entries of the density matrix $\hat{\rho}_{j,k}$. These entries are obtained by measuring in all Pauli operators measurement setting of Equation (3) and using Equation (13) as described above.
3. Fill all the missing entries $\hat{\rho}_{i,j}$ using (15).
4. Perform the singular value decomposition of the density matrix

$$\hat{\rho} = L\Sigma R^{\dagger}, \tag{17}$$

Figure 2 Experimental setup of the low-rank matrix-completion quantum state tomography. The green color represents the entries that are obtained experimentally. The light green color shows only the real part of the entries of the matrix. We first obtain the diagonal entries of the rank-one matrix using computational-basis measurement. Using $U = H$ in the above circuit enables us to obtain the real component of the entries while using $U = S^\dagger H$ provides the Imaginary components of entries

where Σ is a diagonal matrix containing singular values entries on its diagonal as $\lambda_1, \lambda_2, \ldots, \lambda_d$ and L (and R) is the left (and right) orthogonal matrix of dimension d.

5. Shrink the singular values of $\hat{\rho}$ by setting singular-values as

$$\hat{\lambda}_i = \begin{cases} \lambda_i - \lambda_{r+1}, & \text{for } i \leq r \\ 0, & \text{for } i > r \end{cases} \tag{18}$$

where r is the rank of the density matrix and we obtain the new diagonal matrix $\hat{\Sigma}$ with entries $\hat{\lambda}_1, \hat{\lambda}_2, \ldots, \hat{\lambda}_d$. Since a pure state in quantum mechanics has a density matrix with only one non-zero eigenvalue, its rank is equal to 1, meaning $r = 1$.

6. Replace diagonal matrix Σ with $\hat{\Sigma}$ to obtain

$$\hat{\sigma} = L\hat{\Sigma}R^\dagger. \tag{19}$$

7. Update only the missing entries while keeping the entries obtained from measurement unchanged

$$\hat{\rho}(\Delta) = \hat{\sigma}(\Delta), \quad \forall (i,j) \in \Delta. \tag{20}$$

8. Repeat steps 4-7 until $\|\hat{\rho}_{\text{iter}} - \hat{\rho}_{\text{iter}-1}\|_F \leq \epsilon$, where ϵ is some tolerence, is reached either after p times or after K iterations.

A schematic diagram of the experimentally obtained density matrix is shown in Fig. 2 where

$$H = \frac{1}{\sqrt{2}} \begin{bmatrix} 1 & 1 \\ 1 & -1 \end{bmatrix}, \quad \text{and} \quad S^\dagger = \begin{bmatrix} 1 & 0 \\ 0 & e^{-\frac{i\pi}{2}} \end{bmatrix}. \tag{21}$$

and the complete procedure is outlined in Algorithm 1. The convergence of this iterative approach is discussed in [37–39], which addresses the norm minimization problem. Here, the iterative process is governed by two main stopping criteria:

Algorithm 1: Pure State Quantum Tomography by Matrix Completion

Input: N copies of the n-qubit pure state $|\psi\rangle$.

Input: ϵ

Input: Patience

Output: Estimate $|\hat{\psi}\rangle$ of $|\psi\rangle$

1　$\hat{\rho}_{i,i} \leftarrow |\langle \psi | i \rangle|^2,$ 　　　　　　　　　▶ Computational basis measurement

2　**for** $i \in 1 \to n$ **do**

3　　**for** $x \in 1 \to 2$ **do**

4　　　$\Lambda_x^i \leftarrow I_2^{\otimes i-1} \otimes \sigma_x^i \otimes I_2^{\otimes n-i},$ 　　　▶ Pauli operators

5　　　$|V_{x,\pm 1}^{2^i \nu + \zeta, 2^i \nu + \zeta + 2^{i-1}}\rangle \leftarrow \text{eig}(\Lambda_x^i),$ 　　▶ where $\nu \in \mathbb{Q}_{\frac{d}{2^i}}$ and $\zeta \in \mathbb{Q}_{2^{i-1}}$

6　　　$\Pi_{x,\pm 1}^{j,k} \leftarrow |V_{x,\pm 1}^{j,k}\rangle \langle V_{x,\pm 1}^{j,k}|,$ 　　　▶ where $j = 2^i \nu + \zeta$ and $k = 2^i \nu + \zeta + 2^{i-1}$

7　　　$\hat{p}_{x,\pm 1}^{j,k} \leftarrow \langle \psi | \Pi_{x,\pm 1}^{j,k} | \psi \rangle,$ 　　　▶ Local Pauli measurements

8　　$\hat{\rho}_{j,k} \leftarrow \frac{1}{2}(-\hat{p}_{1,-1}^{j,k} + \hat{p}_{1,1}^{j,k} - i\hat{p}_{2,-1}^{j,k} + i\hat{p}_{2,1}^{j,k}),$ 　▶ Density matrix entries

9　　$\hat{\rho}_{k,j} \leftarrow \hat{\rho}_{j,k}^\dagger,$ 　　　　　　　▶ Hermitian symmetric

10　$\hat{\rho}(\Delta) = \text{mean}(\hat{\rho}_{\cdot,j}),$ 　　　　　▶ for all missing entries in Δ

11　p $\leftarrow 0$

12　**for** iter $\in 1 \to K$ **do**

13　　$L, \Sigma, R^\dagger \leftarrow \text{svd}(\hat{\rho}_{\text{iter}})$ 　　　　▶ Singular value decomposition

14　　**if** $i \leq 1$ **then**

15　　　$\hat{\Sigma}_{1,1} \leftarrow \lambda_1 - \lambda_2$ 　　　　▶ Shrink singular values

16　　**else**

17　　　$\hat{\Sigma}_{i,i} \leftarrow 0$

18　　$\hat{\sigma} \leftarrow L\hat{\Sigma}R^\dagger$ 　　　　　　　▶ Singular value decomposition

19　　$\hat{\rho}_{iter}(\Delta) = \hat{\sigma}(\Delta)$ 　　　　　▶ Update the missing values

20　　**if** $\|\hat{\rho}_{\text{iter}} - \hat{\rho}_{\text{iter}-1}\|_F \leq \epsilon$ **then**

21　　　p $\leftarrow$ p + 1

22　　**if** $p = $ *Patience* **then**

23　　　break

24　$|\hat{\psi}\rangle \leftarrow \text{eig}(\hat{\rho}_{\text{iter}}),$ 　　　　　▶ Eigenvector with highest eigenvalue

25　**return** $|\hat{\psi}\rangle$

- *Tolerance:* A predefined threshold for the Frobenius norm of the difference between successive density matrix estimates, ensuring that iterations continue until the estimate stabilizes within this threshold.
- *Patience:* A limit on the number of iterations to perform without significant improvement, preventing endless iteration in cases of slow convergence.

Our proposed algorithm demonstrates effective performance across a broad spectrum of quantum states. However, the algorithm struggles to reconstruct excessively sparse quantum states. It can accurately reconstruct Greenberger-Horne-Zeilinger (GHZ) states of the form $|\phi_1\rangle = \frac{|0\rangle^{\otimes n} + |1\rangle^{\otimes n}}{\sqrt{2}}$, but it encounters difficulties with states like $|\phi_2\rangle = \frac{|0\rangle^{\otimes n} + i|1\rangle^{\otimes n}}{\sqrt{2}}$, failing to account for the imaginary component. We obtain the same density matrix from the reconstruction of the $|\phi_1\rangle$ and $|\phi_2\rangle$ states.

3 Results

To gauge the accuracy of state tomography, we use the common figure of merit, infidelity, which characterizes the distance between these states. Infidelity is defined as

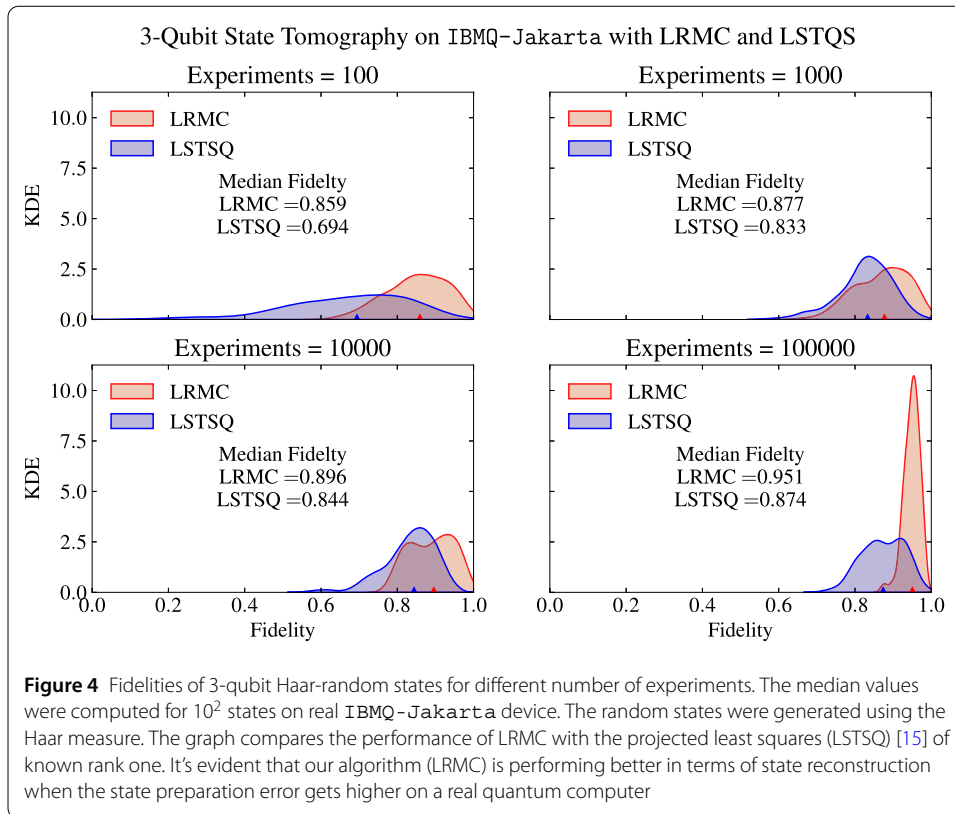$$1 - F(\rho, \sigma) = 1 - (\text{tr}\sqrt{\sqrt{\sigma}\rho\sqrt{\sigma}})^2, \tag{22}$$

where $F(\rho, \sigma)$ is the fidelity between ρ and σ.

Our proposed algorithm is compared to two existing techniques, the five-basis method, and the scalable estimation method, in order to evaluate its performance. The five-basis method employs entangled basis measurements to reconstruct pure quantum states, while the scalable estimation method relies on local basis measurements. To assess the accuracy of each method, we generated 10^2 randomly selected pure quantum states according to the Haar distribution, with n varying from 2 to 5, and plotted the median infidelity as a function of the number of shots for each. The comparison of these experimental simulated results is demonstrated in Fig. 3 and shows that our algorithm outperforms both the five-basis and scalable estimation methods, as it exhibits lower median infidelity.
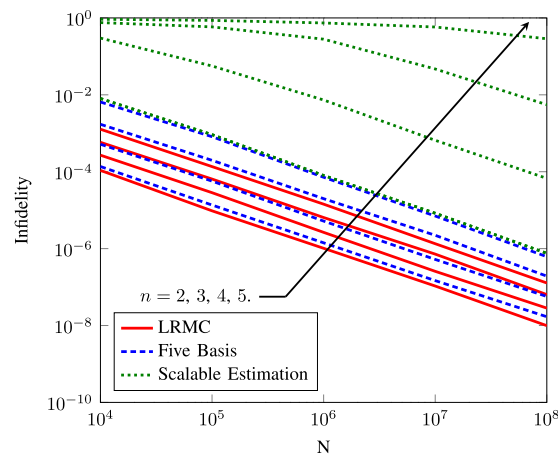
Figure 3 Median Infidelities of 10^2 randomly generated pure state of qubits $n = 2, 3, 4, 5$ from LRMC (proposed), Scalable Estimation [33] and Five Basis [27] as a function of a number of total measurements. The performance of LRMC improves as compared to the Scalable Estimation and Five Basis as the number of qubits increases
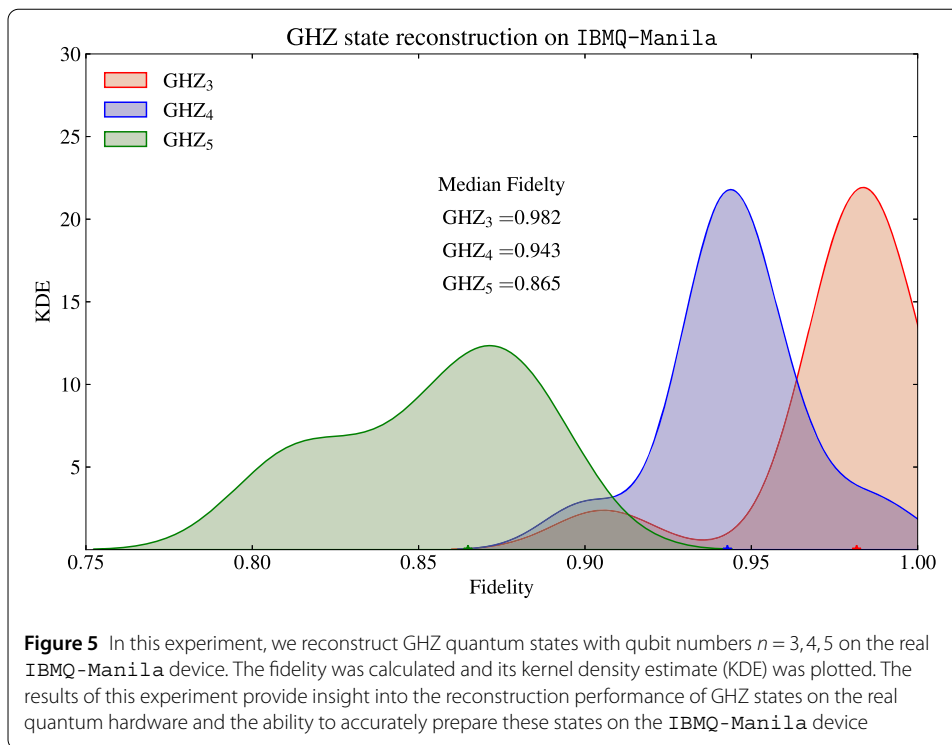
Figure 4 Fidelities of 3-qubit Haar-random states for different number of experiments. The median values were computed for 10^2 states on real `IBMQ-Jakarta` device. The random states were generated using the Haar measure. The graph compares the performance of LRMC with the projected least squares (LSTSQ) [15] of known rank one. It's evident that our algorithm (LRMC) is performing better in terms of state reconstruction when the state preparation error gets higher on a real quantum computer

Our technique has been experimentally verified using a 7-qubit `IBMQ-Jakarta` superconducting quantum computer [40]. This device, with average measurement and CNOT errors of $2.220e^{-2}$ and $7.511e^{-3}$ respectively, is used to implement our algorithm. The circuit design, shown in Fig. 2, is used to generate 10^2 Haar-random pure three-qubit states on the real `IBMQ-Jakarta` device. The median fidelity results are then plotted as a kernel density estimate (KDE) in Fig. 4, along with the least square with known rank one projection. These numerical results demonstrate the precision of our algorithm in benchmarking cloud-based IBM quantum devices, as compared to the projected least square.

We observe that the state preparation error associated with generating random quantum states on a real quantum computer becomes increasingly dominant as the number of qubits increases. To overcome this challenge, we utilized GHZ states, which are a class of entangled quantum states that are easy to prepare on real quantum hardware. An n-qubit GHZ state is shown as

$$|GHZ\rangle = \frac{|0\rangle^{\otimes n} + |1\rangle^{\otimes n}}{\sqrt{2}}. \tag{23}$$

In Fig. 5, we employ a different device, `IBMQ-Manila`, for our experiment. The KDE of the median fidelity for 11 GHZ states with $n = 3, 4, 5$ qubits is plotted, using 2^{13} shots. This device has an average readout and CNOT error of $2.110e^{-2}$ and $6.33e^{-3}$, respectively. Our algorithm is able to reconstruct GHZ states with a median fidelity of over 86% for up to five qubits on real IBM devices.

Figure 5 In this experiment, we reconstruct GHZ quantum states with qubit numbers $n = 3, 4, 5$ on the real `IBMQ-Manila` device. The fidelity was calculated and its kernel density estimate (KDE) was plotted. The results of this experiment provide insight into the reconstruction performance of GHZ states on the real quantum hardware and the ability to accurately prepare these states on the `IBMQ-Manila` device

4 Conclusion

The proposed algorithm in this paper offers a significant advancement in the estimation of pure states on NISQ devices. By relying on local measurements and local gates, it provides a computationally efficient solution that is less susceptible to errors and decoherence. The implementation of local Pauli bases with simple gates such as H and S contributes to the improved accuracy of the algorithm. Additionally, the reduced circuit depth of the algorithm can have a crucial impact in mitigating the negative effects of gate errors and decoherence that are prevalent in real quantum devices. Overall, this algorithm for estimating pure states has the potential to play a crucial role in improving the accuracy of estimation and benchmarking tasks on NISQ devices. Moreover, its possible extension to mixed states through carefully designed measurements and higher rank approximations could further enhance its applicability in quantum computing. Thus, this algorithm holds great promise for advancing the capabilities of NISQ devices and bringing us closer to practical quantum computing applications.

Data availability
The source code of the numerical and experimental generated data that support the findings of this study are available from the corresponding author upon reasonable request.

Declarations

Competing interests
The authors declare no competing interests.

Author details
[1]Department of Electronics and Information Convergence Engineering, Kyung Hee University, 1732 Deogyeong-daero, Yongin-si, Gyeonggi-do 17104, Korea. [2]Department of Electrical Engineering and Automation, Aalto University, Espoo, 02150, Finland. [3]Interdisciplinary Centre for Security, Reliability and Trust (SnT), Univerity of Luxembourg, L-1855, Luxembourg. [4]Department of Electrical and Computer Engineering, Memorial University of Newfoundland, St. John's, NL, Canada.

References
1. Preskill J. Quantum computing in the NISQ era and beyond. Quantum. 2018;2:79.
2. Kandala A, Mezzacapo A, Temme K, Takita M, Brink M, Chow JM, Gambetta JM. Hardware-efficient variational quantum eigensolver for small molecules and quantum magnets. Nature. 2017;549(7671):242–6.
3. Zhang J, Pagano G, Hess PW, Kyprianidis A, Becker P, Kaplan H, Gorshkov AV, Gong Z-X, Monroe C. Observation of a many-body dynamical phase transition with a 53-qubit quantum simulator. Nature. 2017;551(7682):601–4.
4. Loss D, DiVincenzo DP. Quantum computation with quantum dots. Phys Rev A. 1998;57:120–6.
5. Bernien H, Schwartz S, Keesling A, Levine H, Omran A, Pichler H, Choi S, Zibrov AS, Endres M, Greine M, et al. Probing many-body dynamics on a 51-atom quantum simulator. Nature. 2017;551(7682):579–84.
6. Reck M, Zeilinger A, Bernstein HJ, Bertani P. Experimental realization of any discrete unitary operator. Phys Rev Lett. 1994;73:58–61.
7. Terhal BM. Quantum supremacy, here we come. Nat Phys. 2018;14(6):530–1.
8. Madsen LS, Laudenbach F, Askarani MF, Rortais F, Vincent T, Bulmer JF, Miatto FM, Neuhaus L, Helt LG, Collins MJ, et al. Quantum computational advantage with a programmable photonic processor. Nature. 2022;606(7912):75–81.
9. Arute F, Arya K, Babbush R, Bacon D, Bardin JC, Barends R, Biswas R, Boixo S, Brandao FG, Buell DA, et al. Quantum supremacy using a programmable superconducting processor. Nature. 2019;574(7779):505–10.
10. Eisert J, Hangleiter D, Walk N, Roth I, Markham D, Parekh R, Chabaud U, Kashefi E. Quantum certification and benchmarking. Nat Rev Phys. 2020;2(7):382–90.
11. Torlai G, Melko RG. Machine-learning quantum states in the NISQ era. Annu Rev Condens Matter Phys. 2020;11(1):325–44.
12. Shabani A, Kosut RL, Mohseni M, Rabitz H, Broome MA, Almeida MP, Fedrizzi A, White AG. Efficient measurement of quantum dynamics via compressive sensing. Phys Rev Lett. 2011;106:100401.
13. Lloyd S, Mohseni M, Rebentrost P. Quantum principal component analysis. Nat Phys. 2014;10(9):631–3.
14. Banaszek K, D'Ariano GM, Paris MGA, Sacchi MF. Maximum-likelihood estimation of the density matrix. Phys Rev A. 1999;61:010304.
15. Opatrný T, Welsch D-G, Vogel W. Least-squares inversion for density-matrix reconstruction. Phys Rev A. 1997;56:1788–99.
16. Qi B, Hou Z, Li L, Dongi D, Xiang G, Guo G. Quantum state tomography via linear regression estimation. Sci Rep. 2013;3:3496.
17. Blume-Kohout R. Optimal, reliable estimation of quantum states. New J Phys. 2010;12(4):043034.
18. Dodonov VV, Man'ko VI. Positive distribution description for spin states. Phys Lett A. 1997;229(6):335–9.
19. Amiet J-P, Weigert S. Reconstructing a pure state of a spinsthrough three Stern-Gerlach measurements. J Phys A, Math Gen. 1999;32(15):2777–84.
20. Steffens A, Riofrío CA, McCutcheon W, Roth I, Bell BA, McMillan A, Tame MS, Rarity JG, Eisert J. Experimentally exploring compressed sensing quantum tomography. Quantum Sci Technol. 2017;2(2):025005.
21. Kueng R, Rauhut H, Terstiege U. Low rank matrix recovery from rank one measurements. Appl Comput Harmon Anal. 2017;42(1):88–116.
22. Bolduc E, Knee GC, Gauger EM, Leach J. Projected gradient descent algorithms for quantum state tomography. npj Quantum Inf. 2017;3(1):1–9.
23. Wootters WK, Fields BD. Optimal state-determination by mutually unbiased measurements. Ann Phys. 1989;191(2):363–81.
24. Adamson RBA, Steinberg AM. Improving quantum state estimation with mutually unbiased bases. Phys Rev Lett. 2010;105:030406.
25. Cramer M, Plenio MB, Flammia ST, Somma R, Gross D, Bartlett SD, Landon-Cardinal O, Poulin D, Liu Y-K. Efficient quantum state tomography. Nat Commun. 2010;1(1):1–7.
26. Tóth G, Wieczorek W, Gross D, Krischek R, Schwemmer C, Weinfurter H. Permutationally invariant quantum tomography. Phys Rev Lett. 2010;105:250403.
27. Goyeneche D, Cańas G, Etcheverry S, Gómez ES, Xavier GB, Lima G, Delgado A. Five measurement bases determine pure quantum states on any dimension. Phys Rev Lett. 2015;115:090401.
28. Carmeli C, Heinosaari T, Kech M, Schultz J, Toigo A. Stable pure state quantum tomography from five orthonormal bases. Europhys Lett. 2016;115(3):30001.
29. Zambrano L, Pereira L, Martínez D, Cańas G, Lima G, Delgado A. Estimation of pure states using three measurement bases. Phys Rev Appl. 2020;14:064004.

30. Rambach M, Qaryan M, Kewming M, Ferrie C, White AG, Romero J. Robust and efficient high-dimensional quantum state tomography. Phys Rev Lett. 2021;126:100402.
31. Ferrie C. Self-guided quantum tomography. Phys Rev Lett. 2014;113:190404.
32. Chapman RJ, Ferrie C, Peruzzo A. Experimental demonstration of self-guided quantum tomography. Phys Rev Lett. 2016;117:040402.
33. Pereira L, Zambrano L, Delgado A. Scalable estimation of pure multi-qubit states. npj Quantum Inf. 2022;8(1):1–12.
34. Strang G. In: Linear algebra and learning from data 1(1). 2019. p. 413–28.
35. Eckart C, Young G. The approximation of one matrix by another of lower rank. Psychometrika. 1936;1(3):211–8.
36. Kumar NK, Schneider J. Literature survey on low rank approximation of matrices. Linear Multilinear Algebra. 2017;65(11):2212–44.
37. Troyanskaya O, Cantor M, Sherlock G, Brown P, Hastie T, Tibshirani R, Botstein D, Altman RB. Missing value estimation methods for DNA microarrays. Bioinformatics. 2001;17(6):520–5.
38. Cho M. Imputation of missing values by low rank matrix approximation. US Bureau of Labor Statistics 2021.
39. Cai J-F, Cand'es EJ, Shen Z. A singular value thresholding algorithm for matrix completion. SIAM J Optim. 2010;20(4):1956–82.
40. 7-qubit backend: IBM Q team, IBM Q 7 Jakarta backend specification v1.2.5. (Accessed: Jan 2023).

Publisher's Note